Metamagnetism and tricritical behavior in the Kondo lattice model

B. H. Bernhard*

Departamento de Física, Universidade do Estado de Santa Catarina, 89.219-710 Joinville, SC, Brazil

(Received 30 June 2022; revised 22 August 2022; accepted 23 August 2022; published 30 August 2022)

The phase diagram of the Kondo lattice model is explored around the ferromagnetic region, including an external magnetic field, and allowing the coexistence of ferromagnetism and Kondo effect (FM+K). Considering the combined effect of temperature and pressure, the evolution of the FM+K phase yields a wing structure phase diagram with a tricritical point and a ferromagnetic quantum critical end point. The evolution of the spin-selective Kondo insulator phase, inside the coexistence region, introduces another critical end point. The results show a correspondence with the experimental phase diagram of heavy-fermion compounds, in particular, the ferromagnetic superconductor UGe_2.

DOI: 10.1103/PhysRevB.106.054436

I. INTRODUCTION

The Kondo lattice model (KLM) [1–5] constitutes a consolidated framework to explain the properties of heavy-fermion systems, including a number of cerium, ytterbium, and uranium compounds. The underlying physics is governed by the competition between magnetic order and the Kondo effect depicted in the Doniach's diagram, which allows a direct comparison with experimental phase diagrams of temperature versus pressure [6–8]. Current interest in the model encompasses the study of quantum criticality [9–11], the prospection of novel phases, involving charge order (around quarter filling) [12–14], partial Kondo screening [15,16], the exhaustion problem (in the low concentration limit) [17–19], the interplay of magnetism and Kondo effect with geometric frustration [20,21], the existence of incommensurate spin density waves or spiral magnetic states [22,23], the role of impurity concentration in Kondo alloys [24], and the coexistence of ferromagnetism with unconventional superconductivity [25–28].

The ground-state phase diagram of the KLM as a function of the Kondo coupling J_K and electron concentration n as well as the finite-temperature phase diagram, can be derived within the fermionic mean-field approach. It includes pure ferromagnetic (FM), antiferromagnetic, Kondo (K), and paramagnetic (PM) phases and admits the coexistence of magnetic order and Kondo effect [29–32]. Here we will focus on the ferromagnetic region of the phase diagram, with concentrations n around $1/8$ filling. As previously described [32], the coexistence region (FM+K) can be subdivided into two portions, namely, a spin selective Kondo insulator (SSKI) phase and an intermediate weak ferromagnetic phase (FMK). The model has also been addressed by other reputable theoretical methods, such as quantum or variational Monte Carlo [33–35], and dynamical mean-field theory [24,36–38], which qualitatively corroborate the phase diagram obtained in the simplified mean-field picture.

The KLM is fundamentally connected to the Anderson lattice model (ALM) describing hybridized f and c bands where valence fluctuations are allowed [2,4,39,40]. The pure and mixed phases mentioned above are also present in the phase diagram of the ALM as a function of the hybridization V, the position of the f-electron level E_f, and local Coulomb repulsion U as can be obtained from different methods [41–43]. These studies also suggest an appropriate interpretation for some well-known shortcomings of the fermionic mean-field description, such as, the behavior of the order parameter $\langle\lambda\rangle$ (to be introduced in the next section) characteristic of the Kondo phase. However, the pressure dependence of the model parameters V and E_f are still controversial in the ALM.

In connection to an extensive experimental investigation, the KLM applies to a variety ferromagnetic Ce-based [6,11,44] and Yb-based compounds [45,46]. The metamagnetism in Kondo systems has been investigated in Refs. [36,47,48] where the magnetization curves may exhibit a plateau as a function of magnetic-field B. In the case of ferromagnetic compounds, the corresponding plateau is reminiscent of the SSKI phase appearing in the ground-state phase diagram in the absence of B. Owing to the possible coexistence of ferromagnetism and Kondo effect, the KLM may be also pertinent to uranium compounds without necessarily incorporating orbital degeneracy [49].

The itinerant ferromagnet UGe_2 exhibits two ferromagnetic phases FM1 and FM2 (with small and large magnetic moments, respectively), and a superconducting phase at low temperature near the boundary between these two magnetic phases [50–53]. The experimental phase diagram of this compound is characterized by wing-shaped surfaces of first-order transitions between the FM1 and the paramagnetic phases, delimited by lines of second-order transitions starting at a tricritical point (TCP) and terminating at a quantum critical end point (QCEP). The FM1-FM2 transition is first order at low temperatures, but it is converted to a broad crossover above a critical end point CEP.

*benhur.bernhard@udesc.br

Wing-structure phase diagrams are universally observed in itinerant ferromagnets [54] and can be qualitatively reproduced from the Stoner theory, assuming a single-band density of states with a positive curvature in the neighborhood of the Fermi level [28,55]. The corresponding results are compatible with the Wolfarth-Rhodes-Shimizu (WRS) theory based on phenomenological Landau expansions [56,57]. A generalized expansion of the free energy has been proposed in Ref. [58], incorporating the many-body effect associated with particle-hole excitations. In the latter picture, the wing shape of the phase diagram can be obtained independent of details in the band structure.

The essential role of the Kondo hybridization in UGe_2 has been recently reinforced by the observation of a Kondo resonance in this compound [59], stimulating an appropriate explanation of its phase diagram from microscopic models of heavy fermions. A detailed theoretical investigation of the critical behavior observed in UGe_2 was performed in Ref. [60] based on the ALM, which provides an improved fitting of the observed phase diagram in comparison with the other methods mentioned above. As we demonstrate here, a similar phase diagram can be obtained directly from the KLM.

In this paper, we study the evolution of the phase diagram as a function of temperature T, Kondo coupling J_K, and applied magnetic-field B, revealing the critical behavior exhibited by the KLM. In the next section, we review the decoupling method introduced in Ref. [32] for the KLM. In Sec. III, we present the results obtained from the evolution of the order parameters and the corresponding phase diagram. In the past section, we compare our results with previous theoretical works and experimental observations.

II. MODEL AND APPROXIMATION

The Kondo lattice Hamiltonian in presence of an uniform magnetic-field B can be written as a sum of three terms,

$$\mathcal{H} = \mathcal{H}_t + \mathcal{H}_K + \mathcal{H}_h, \tag{1}$$

where the first one represents a tight-binding conduction band,

$$\mathcal{H}_t = -\sum_{ij\sigma} t_{ij}\, c^\dagger_{i\sigma} c_{j\sigma}. \tag{2}$$

The localized spins $\mathbf{S}_i$ are represented by the pseudofermion operators $f^\dagger_{i\sigma}, f_{i\sigma}$, subject to the constraint $\langle n_f\rangle = \sum_\sigma \langle n^f_{i\sigma}\rangle = 1$. Following Ref. [32], we write the second term in Eq. (1) in the form

$$\mathcal{H}_K = -J_K \sum_{i\sigma} \lambda_{i\bar\sigma}\lambda_{i\sigma} - J_K/2 \sum_{i\sigma} n^f_{i\bar\sigma} n^c_{i\sigma}, \tag{3}$$

by introducing the operator,

$$\lambda_{i\sigma} = 1/2(f^\dagger_{i\sigma} c_{i\sigma} + c^\dagger_{i\sigma} f_{i\sigma}). \tag{4}$$

The magnetic field is included in the last term of 1,

$$\mathcal{H}_h = -h \sum_i \left(m^c_i + m^f_i\right), \tag{5}$$

where $m^f_i = 2S^z_i = n^f_{i\uparrow} - n^f_{i\downarrow}$ and $m^c_i = 2s^z_i = n^c_{i\uparrow} - n^c_{i\downarrow}$ are the local magnetization operators and $h = \mu_B B$ (for spin $S = 1/2$).

The fermionic mean-field approximation [32] yields an effective Hamiltonian,

$$\mathcal{H}' = \mathcal{H}_t + \mathcal{H}_{\tilde V} + \mathcal{H}_f + \mathcal{H}'_h, \tag{6}$$

where

$$\mathcal{H}_{\tilde V} = -\sum_{i\sigma} \tilde V_{i\sigma}(f^\dagger_{i\sigma} c_{i\sigma} + c^\dagger_{i\sigma} f_{i\sigma}), \tag{7}$$

$$\mathcal{H}_f = E_f \sum_{i\sigma} n^f_{i\sigma}, \tag{8}$$

and

$$\mathcal{H}'_h = \sum_{i\sigma} \sigma\left(h^f_i - h\right) n^f_{i\sigma} + \sum_{i\sigma} \sigma\left(h^c_i - h\right) n^c_{i\sigma}, \tag{9}$$

using $\sigma = +$ (or $-$) for up (or down) spin. The effective hybridizations in Eq. (7) are given by $\tilde V_{i\sigma} = J_K\langle\lambda_{i\bar\sigma}\rangle$. Magnetic long-range order is related to the molecular-fields $h^f_i = \frac{1}{2}J_K\langle s^z_i\rangle$ and $h^c_i = \frac{1}{2}J_K\langle S^z_i\rangle$, which imply a magnetic coupling between local and itinerant moments. The chemical potential μ is fixed from the condition $\sum_\sigma \langle n^c_{i\sigma}\rangle = n$, where n is the conduction electron concentration. In Eq. (8), E_f plays the role of a Lagrange multiplier, determined by the constraint $\langle n_f\rangle = 1$. The parameters E_f and $\tilde V_{i\sigma}$ must be distinguished from the f-electron level and the bare hybridization parameters appearing in the context of the Anderson lattice model. The self-consistent evaluation of E_f and μ partially restores the correlation effects present in our starting Hamiltonian in Eq. (1) that have been neglected in the mean-field decoupling.

In the fermionic mean-field approach, magnetism and the Kondo effect are characterized, respectively, by the magnetizations $\langle S^z_i\rangle$, $\langle s^z_i\rangle$, and by the averages $\langle\lambda_{i\sigma}\rangle$, which are all evaluated as integrals over their corresponding (nonrigid band) densities of states or spectral functions multiplied by the Fermi function. In the pure phases FM and K, only the respective order parameters are present, whereas in the PM phase all of them are equal to zero. On the other hand, when all order parameters acquire a finite value, the system shows a stable phase with coexistence (FM+K). As confirmed by the calculations, the FM+K region can be further subdivided into two solutions: SSKI, characterized by a plateau in the total magnetization $S^z_t = \langle S^z_i\rangle + \langle s^z_i\rangle$, and FMK, where S^z_t decreases monotonically for increasing J_K or temperature.

III. RESULTS

In this section, we choose an electron concentration $n = 0.25$, which corresponds to a 1/8-filled conduction band and take the hopping parameter t as the energy unit. The variation of the order parameters as a function of J_K/t in the presence of a magnetic-field h in the low-temperature limit is shown in Fig. 1. At low values of J_K, the system is stabilized in a pure FM phase, where $\langle\lambda_{i\sigma}\rangle = 0$ and the local spin average $\langle S^z_i\rangle$ reaches its saturation value. We also observe that the contribution of the conduction electron spin $\langle s^z_i\rangle$ to the total magnetization is much smaller and opposite. By increasing J_K above a threshold value J_λ, a discontinuous transition occurs to a region with coexistence of ferromagnetic order and Kondo effect where all presupposed order parameters are different from zero.

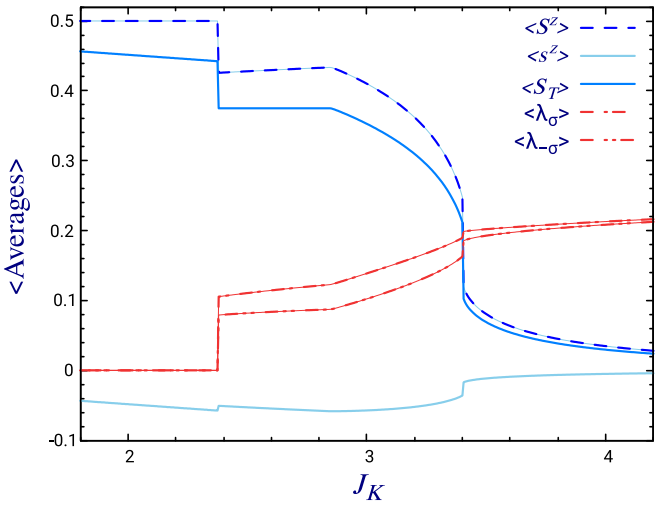

FIG. 1. Magnetizations $\langle S_i^z \rangle$, $\langle s_i^z \rangle$, and S_t^z, and the averages $\langle \lambda_{i\sigma} \rangle$ as a function of J_K/t for $n = 0.25$ with a magnetic-field $h = 0.005t$ at a low temperature $T = 0.0001t$.

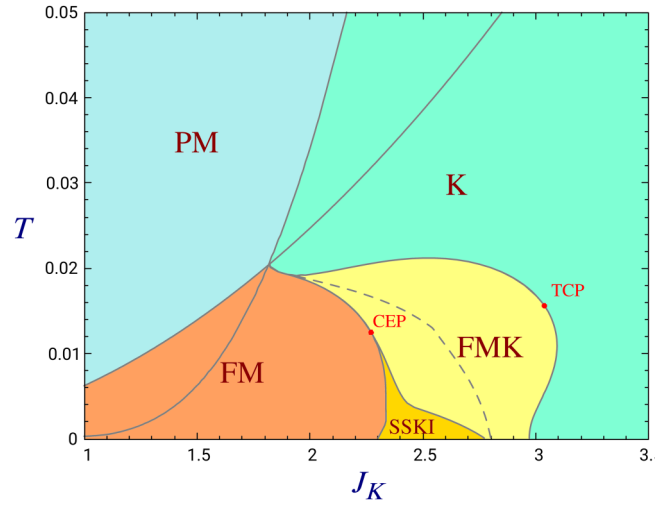

FIG. 3. J_K-T phase diagram for $h = 0$. The nature of the phase transitions and the special points are discussed in the text. We also show the prolongation of the boundary lines between the pure phases FM/PM and K/PM, which mark the presence of the K and FM solutions. The dashed line represents the interface FM/K obtained from the calculated Gibbs free energies.

The coexistence region can be subdivided into three parts. For $J_\lambda < J_K < J_p$, the system is in the SSKI phase with a plateau in the total magnetization $S_t^z = (1-n)/2$, and a Fermi level located in a gap of the majority spin density of states. For $J_K > J_p$, S_t^z decreases monotonically. In presence of a magnetic-field h, the magnetizations do not vanish so that the phase coexistence extends to larger values of J_K. The transition from the intermediate FMK phase to the extended K phase is marked by a discontinuity of the magnetizations at $J_K = J_\delta$.

The behavior of S_t^z is shown in Fig. 2 as a function of J_K and h where the two mentioned discontinuities appear as vertical surfaces, which can be projected onto the J_K-h plane. The phase boundary between the FMK and the K phases shifts to higher values of J_K for increasing h. The discontinuity δS_t^z of S_t^z at $J_K = J_\delta$ draws a line of first-order transitions in the J_K-h phase diagram, ending up at a critical point (CP) where

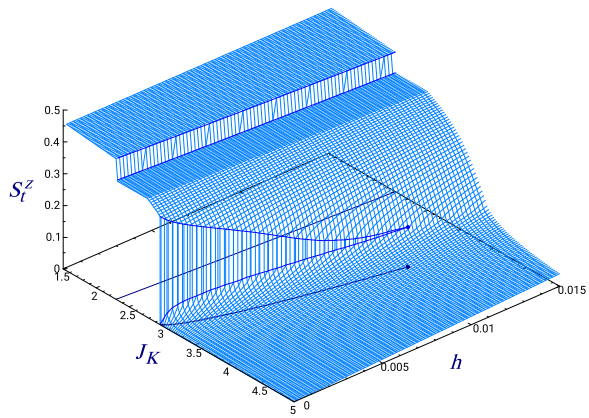

FIG. 2. Total magnetization S_t^z as a function of J_K/t and h/t at $T = 0.0001t$. The surface is drawn with fixed increments in both axes for better visibility. The borders of the vertical discontinuities are superposed as smoother curves. The horizontal projection of these curves provides the transition line in the h-J_K diagram.

δS_t^z goes to zero. A continuation of this line above the CP can be defined from the minimum of the derivative of S_t^z. On the other hand, the discontinuities of the averages at $J_K = J_\lambda$ at the boundary between FM and FM+K phases are practically unaffected by the magnetic field as well as the width of the plateau of the SSKI phase, which persist for higher values of h.

The borders of these allowed phases can be delimited by the vanishing of the order parameters, which may occur as continuous (second-order) or discontinuous (first-order) transitions. As usually admitted in mean-field treatments, the phase transitions related to the vanishing of $\langle \lambda \rangle$ should be interpreted as crossovers. A preliminary draft of the finite temperature phase diagram can be drawn as usually by comparing the pure phases FM, K, and PM, wherever they are competing. The interface FM/K should be determined by the crossing of the corresponding Gibbs free energies $G = E - TS$, which involve the evaluation of the entropies $S(T)$ of the two phases by integration (the same method utilized, e.g., in Ref. [55]).

However, the FM+K region develops somewhere around the FM/K boundary so that the actual phase boundaries should be obtained by numerically analyzing the survival of the FM+K solution. In the coexistence region, it is assumed that the the value of G is lower in the mixed phase as compared to the pure K and FM phases. The self-consistent determination of the order parameters naturally provides the correct stable phases which minimize the Gibbs free energy.

The calculated J_K-T phase diagram is illustrated in Fig. 3 for $h = 0$. The boundaries K/PM and FM/PM are lines of continuous transitions where the respective order parameters (either $\langle \lambda_{i\sigma} \rangle$ or the magnetizations) go to zero. On the other hand, the border between the FM phase and the coexistence region FM+K or the pure K phase is a line of discontinuous transitions where the value of $\langle \lambda_{i\sigma} \rangle$ drops to zero at decreasing J_K, accompanied by jumps in the magnetizations $\langle S_i^z \rangle$ and $\langle s_i^z \rangle$.

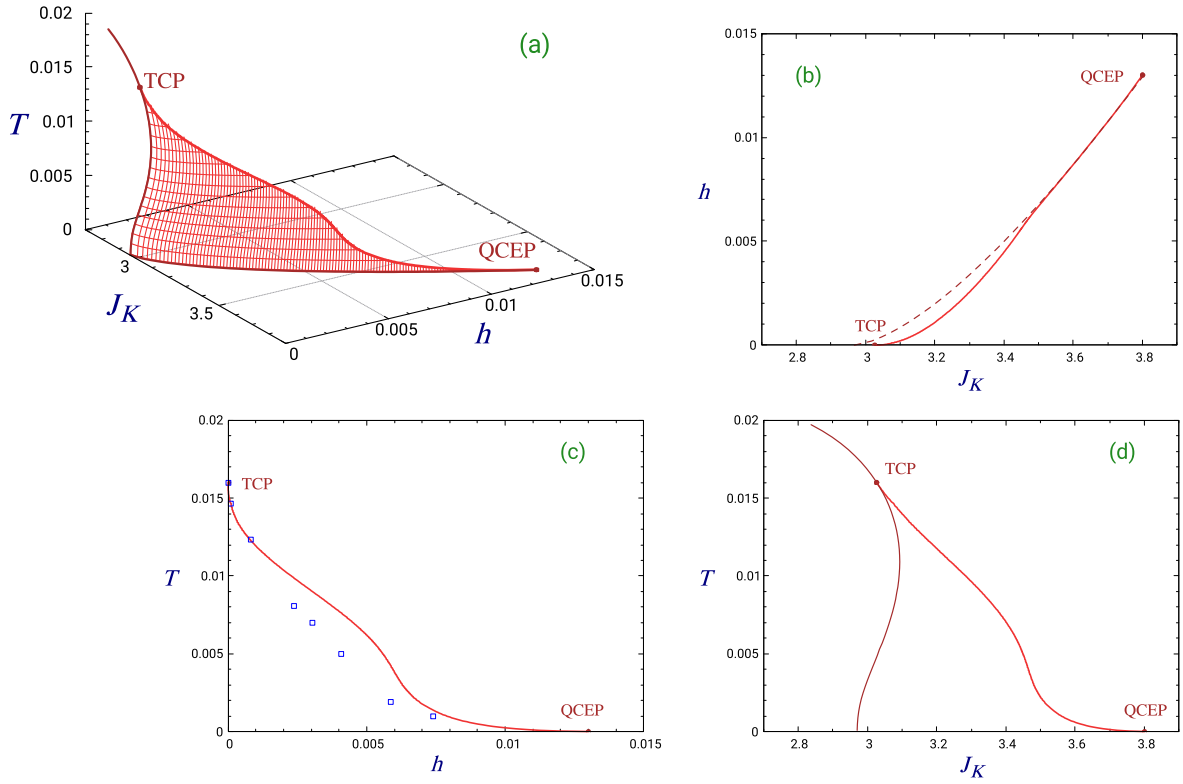

FIG. 4. (a) Wing-structure phase diagram J_K-T-h and the projections of the critical wing line on the planes (b) $h \times J_K$, (c) $T \times h$, and (d) $T \times J_K$. A symmetrical wing is also present in the region $h < 0$.

The boundaries of the SSKI phase are determined by the presence of a magnetization plateau of width Δ related to the Kondo gap in the majority spin density of states [32,38]. Changes in the Fermi surface topology occur at both sides of the SSKI region as the chemical potential crosses this gap. Whereas the discontinuous transition at $J_K = J_\lambda$ is marked by the Kondo breakdown, the transition at J_p consists of a pure Lifshitz transition [43,48]. The value of Δ decreases for increasing T and tends to zero at and tends to zero at CEP where the SSKI phase collapses. Analogously, accompanying the interface FM/FMK above this CEP, another CEP$'$ can be found where the FMK phase also collapses. Between this CEP$'$ and the triple point, a first-order transition can occur directly between the pure FM and K phases. The FMK and K phases are separated by a line of second-order transitions starting at the triple point (intersecting the pure phases K, FM, and PM) and terminating at a TCP. The curvature of this line implies a reentrant behavior of the magnetizations as a function of J_K in a narrow range of temperature around $T = 0.02t$. The FMK/K boundary continues as a line of first-order transitions (on the $h = 0$ plane) with a reentrant behavior from the TCP to the horizontal axis.

In the presence of a magnetic field, we obtain the phase diagram J_K-T-h shown in Fig. 4. It is characterized by two symmetrical wing-shaped surfaces of first-order transitions delimited by lines of critical points that link the TCP (located at $T = 0.0160$, $J_K = 3.027$ in the adopted units) to the respective QCEP on the $T = 0$ plane. These critical lines can be obtained by accompanying the evolution of the critical point in Fig. 2 as a function of temperature. Panel 4(b) shows the projection of these critical lines on the $h \times J_K$ plane. The dashed line in this figure represents the line of first-order transitions separating the K and FMK phases in the ground-state phase diagram. Panel 4(c) shows the projection of the critical line on the $T \times h$ plane. The square symbols correspond to the experimental points of Ref. [52]. In order to allow a direct comparison with our results, we have converted the physical units by taking a temperature $T_{TCP} = 24.0$ K at the TCP, which corresponds to an effective hopping $t = 133$ meV. The long tail in this curve makes it difficult to determine the precise location of the QCEP along the h axis from the numerical calculations. An estimated value of $h/t = 0.0130$ corresponds to a magnetic-field $B = 29.0$ T at the QCEP, very close to the value proposed in Ref. [60]. Panel 4(d) shows the projection of the critical line as seen on the $T \times J_K$ phase diagram. The boundary line representing the interface FMK/K in Fig. 3 is also shown. The region between these curves corresponds to metamagnetic behavior as usually represented when describing itinerant electron metamagnetism in the WRS theory [57].

IV. DISCUSSION

As well established from experiments, in connection with Doniach's diagram, the parameter J_K/t in the KLM increases with pressure P in Ce compounds, and it decreases in Yb compounds, although the functional dependence $P(J_K/t)$ is unknown. In addition, the value of the hopping parameter t, usually taken as the energy unit (both in the KLM and in the ALM), is also supposed to increase with pressure. With these essential limitations in mind, the diagram in Fig. 3

corresponds to a P-T phase diagram of ferromagnetic heavy-fermion materials. In particular, it accounts for the weak ferromagnetic phases found in these compounds well below the Kondo temperature T_K.

The obtained phase diagram is in overall agreement with previous mean-field studies, contributing with more details and some noticeable differences. The region corresponding to the SSKI phase in Fig. 3 is substantially reduced in comparison to Ref. [31] where a constant density of states has been used. This indicates an important influence of the lattice geometry when describing the coexistence FM+K. Here we identify the TCP that separates the FMK/K boundary line into continuous and discontinuous transitions, and two critical end points CEP and CEP′ associated with the SSKI and FMK phases respectively.

By studying the effect of a magnetic field on the FMK/K transition, we obtain the wing-structure phase diagram of Fig. 4. It shows a clear resemblance with the observed phase diagram of UGe_2 [50,51,53], providing an alternative to other studies based on the Anderson lattice [60] or on Landau expansions [57,58]. The FM1 and FM2 phases of this compound correspond, respectively, to the coexistent phase FM+K and the pure FM phase in our notation. The nature of the crossover region reported above the CEP remains to be further investigated as well as the differentiation between the SSKI and the FMK phases inside the FM1 phase.

The critical wing line (CWL) in Fig. 4 satisfies the thermodynamic constraints expressed in Ref. [61]. The projection of the CWL in panel 4(d) becomes tangent to the critical line of the FM/FMK transition at the TCP, and the projections of the CWL in panels 4(b) and 4(c) are tangent to the J_K and T axes at the TCP. We also find that the projection of the CWL in panel 4(b) is tangent to the first-order FMK/K transition line on the $T = 0$ plane at the QCEP. The slopes of the CWL decrease drastically as it approaches the QCEP in panels 4(c) and 4(d). This feature is in good agreement with experiments, in contradistinction with the methods of Refs. [57,58], which yield CWLs perpendicular to the $T = 0$ plane. This peculiar quantum critical behavior may be attributed to the Fermi surface changes across the FMK/K transition which are naturally incorporated in the model and captured by the method. We also note that our wing surfaces remain perpendicular to the $T = 0$ plane, consistent with the thermodynamic constraints at low T discussed in Ref. [62]. A direct quantitative comparison with experiments is suggested in Fig. 4(c) assuming a linear transformation of units in both T and h axes, using t as a single fitting parameter.

To summarize, the application of the fermionic mean-field method to the Kondo lattice model provides a satisfactory description of the electronic and magnetic properties observed in a variety of ferromagnetic heavy-fermion compounds as a function of temperature, pressure, and magnetic field. The nature of the phase transitions and critical behavior in uranium compounds can be specified with an appropriate interpretation, before analyzing the impact of valence fluctuations, f-orbital degeneracy, intersite interactions, or details in the band structure. A straightforward comparison of the present results with the experimental phase diagram of UGe_2 supports the idea that unconventional superconductivity might be associated with the SSKI phase. The obtained phase diagram provides a basis for further studies on the KLM and related models incorporating additional competing phases listed in the Introduction.

ACKNOWLEDGMENTS

I acknowledge fruitful discussions with C. Lacroix and support of Brazilian agencies Fundação de Amparo à Pesquisa do Estado de Santa Catarina (FAPESC) and Coordenação de Aperfeiçoamento de Pessoal de Nível Superior (CAPES).

[1] S. Doniach, The Kondo lattice and weak antiferromagnetism, Physica B+C **91**, 231 (1977).

[2] C. Lacroix and M. Cyrot, Phase diagram of the Kondo lattice, Phys. Rev. B **20**, 1969 (1979).

[3] P. Fazekas and E. Müller-Hartmann, Magnetic and nonmagnetic ground states of the Kondo lattice, Z. Phys. B: Condens. Matter **85**, 285 (1991).

[4] H. Tsunetsugu, M. Sigrist, and K. Ueda, The ground-state phase diagram of the one-dimensional Kondo lattice model, Rev. Mod. Phys. **69**, 809 (1997).

[5] P. Coleman, *Introduction to Many-Body Physics* (Cambridge University Press, Cambridge, UK, 2015).

[6] A. L. Cornelius and J. S. Schilling, High-pressure study of the anomalous ferromagnet $CeRh_3B_2$ to 7 GPa: Comparison with substitutional experiments, Phys. Rev. B **49**, 3955 (1994).

[7] J. R. Iglesias, C. Lacroix, and B. Coqblin, Revisited Doniach diagram: Influence of short-range antiferromagnetic correlations in the Kondo lattice, Phys. Rev. B **56**, 11820 (1997).

[8] B. Coqblin, C. Lacroix, M. A. Gusmão, and J. R. Iglesias, *Band-filling effects on Kondo-lattice properties*, Phys. Rev. B **67**, 064417 (2003).

[9] Q. Si and F. Steglich, Heavy Fermions and Quantum Phase Transitions, Science **329**, 1161 (2010).

[10] Y. Wu, Y. Zhang, F. Du, B. Shen, H. Zheng, Y. Fang, M. Smidman, C. Cao, F. Steglich, H. Yuan, J. D. Denlinger, and Y. Liu, Anisotropic $c - f$ Hybridization in the Ferromagnetic Quantum Critical Metal $CeRh_6Ge_4$, Phys. Rev. Lett. **126**, 216406 (2021).

[11] B. Shen, Y. Zhang, Y. Komijani, M. Nicklas, R. Borth, A. Wang, Y. Chen, Z. Nie, R. Li, X. Lu, H. Lee, M. Smidman, F. Steglich, P. Coleman, and H. Yuan, Strange-metal behaviour in a pure ferromagnetic Kondo lattice, Nature (London) **579**, 51 (2020).

[12] T. Misawa, J. Yoshitake, and Y. Motome, Charge Order in a Two-Dimensional Kondo Lattice Model, Phys. Rev. Lett. **110**, 246401 (2013).

[13] R. Peters, S. Hoshino, N. Kawakami, J. Otsuki, and Y. Kuramoto, Charge order in Kondo lattice systems, Phys. Rev. B **87**, 165133 (2013).

[14] J. E. Hirsch, Strong-coupling expansion of the Kondo lattice model, Phys. Rev. B **30**, 5383 (1984).

[15] C. Lacroix, B. Canals, and M. D. Núñez-Regueiro, Kondo Screening and Magnetic Ordering in Frustrated UNi_4B, Phys. Rev. Lett. **77**, 5126 (1996).

[16] Y. Motome, K. Nakamikawa, Y. Yamaji, and M. Udagawa, Partial Kondo Screening in Frustrated Kondo Lattice Systems, Phys. Rev. Lett. **105**, 036403 (2010).

[17] P. Nozières, Impuretés magnétiques et effet Kondo, Ann. Phys. Fr. **10**, 19 (1985).

[18] P. Nozières, Some comments on Kondo lattices and the Mott transition, Eur. Phys. J. B **6**, 447 (1998).

[19] S. Burdin, A. Georges, and D. R. Grempel, Coherence Scale of the Kondo Lattice, Phys. Rev. Lett. **85**, 1048 (2000).

[20] P. Coleman and A. H. Nevidomskyy, Frustration and the Kondo Effect in Heavy Fermion Materials, J. Low Temp. Phys. **161**, 182 (2010).

[21] B. H. Bernhard, B. Coqblin, and C. Lacroix, Frustration in the Kondo lattice model: Local versus extended singlet phases, Phys. Rev. B **83**, 214427 (2011).

[22] R. Peters and N. Kawakami, Large and small Fermi-surface spin density waves in the Kondo lattice model Phys. Rev. B **92**, 075103 (2015).

[23] N. C. Costa, J. P. Lima, and R. R. dos Santos, Spiral magnetic phases on the Kondo Lattice Model: A Hartree-Fock approach, J. Magn. Magn. Mater. **423**, 74 (2017).

[24] B. Poudel, G. Zwicknagl, C. Lacroix, and S. Burdin, Phase diagrams of Kondo alloys, J. Magn. Magn. Mater. **520**, 167405 (2021).

[25] S. S. Saxena, P. Agarwal, K. Ahilan, F. M. Grosche, R. K. W. Haselwimmer, M. J. Steiner, E. Pugh, I. R. Walker, S. R. Julian, P. Monthoux, G. G. Lonzarich, A. Huxley, I. Sheikin, D. Braithwaite, and J. Flouquet, Superconductivity on the border of itinerant-electron ferromagnetism in UGe_2, Nature (London) **406**, 587 (2000).

[26] A. Huxley, I. Sheikin, E. Ressouche, N. Kernavanois, D. Braithwaite, R. Calemczuk, and J. Flouquet, UGe_2: A ferromagnetic spin-triplet superconductor Phys. Rev. B **63**, 144519 (2001).

[27] C. Pfleiderer and A. D. Huxley, Pressure Dependence of the Magnetization in the Ferromagnetic Superconductor UGe_2, Phys. Rev. Lett. **89**, 147005 (2002).

[28] K. G. Sandeman, G. G. Lonzarich, and A. J. Schofield, Ferromagnetic Superconductivity Driven by Changing Fermi Surface Topology, Phys. Rev. Lett. **90**, 167005 (2003).

[29] Z. Z. Li, M. Zhuang, and M. W. Xiao, Ferromagnetic-paramagnetic phase diagram of the Kondo lattice, J. Phys.: Condens. Matter **8**, 7941 (1996).

[30] G. B. Li, G. M. Zhang, and L. Yu, Kondo screening coexisting with ferromagnetic order as a possible ground state for Kondo lattice systems, Phys. Rev. B **81**, 094420 (2010).

[31] Y. Liu, G. M. Zhang, and L. Yu, Weak ferromagnetism with the Kondo screening effect in the Kondo lattice systems, Phys. Rev. B **87**, 134409 (2013).

[32] B. H. Bernhard and C. Lacroix, Coexistence of magnetic order and Kondo effect in the Kondo-Heisenberg model, Phys. Rev. B **92**, 094401 (2015).

[33] F. F. Assaad, Quantum Monte Carlo Simulations of the Half-Filled Two-Dimensional Kondo Lattice Model Phys. Rev. Lett. **83**, 796 (1999).

[34] H. Watanabe and M. Ogata, Fermi-Surface Reconstruction without Breakdown of Kondo Screening at the Quantum Critical Point, Phys. Rev. Lett. **99**, 136401 (2007).

[35] J. Otsuki, H. Kusunose, and Y. Kuramoto, The Kondo Lattice Model in Infinite Dimensions: II. Static Susceptibilities and Phase Diagram, J. Phys. Soc. Jpn. **78**, 034719 (2009).

[36] K. S. D. Beach and F. F. Assaad, Coherence and metamagnetism in the two-dimensional Kondo lattice model, Phys. Rev. B **77**, 205123 (2008).

[37] R. Peters, N. Kawakami, and T. Pruschke, Spin-Selective Kondo Insulator: Cooperation of Ferromagnetism and the Kondo Effect, Phys. Rev. Lett. **108**, 086402 (2012).

[38] R. Peters and N. Kawakami, Ferromagnetic state in the one-dimensional Kondo lattice model, Phys. Rev. B **86**, 165107 (2012).

[39] B. H. Bernhard, C. Lacroix, J. R. Iglesias, and B. Coqblin, Phase diagram for the Anderson lattice model, Phys. Rev. B **61**, 441 (2000).

[40] B. H. Bernhard and B. Coqblin, Pressure induced valence transitions in the Anderson lattice model, Physica B **404**, 3021 (2009).

[41] B. H. Bernhard and C. Lacroix, Thermodynamics of the Anderson lattice, Phys. Rev. B **60**, 12149 (1999).

[42] M. M. Wysokiński, M. Abram, and J. Spałek, Ferromagnetism in UGe_2: A microscopic model, Phys. Rev. B **90**, 081114(R) (2014).

[43] K. Kubo, Lifshitz Transitions in Magnetic Phases of the Periodic Anderson Model J. Phys. Soc. Jpn. **84**, 094702 (2015).

[44] D. P. Rojas, J. I. Espeso, J. Rodriguez Fernandez, J. C. Gomez Sal, J. Sanchez Marcos, and H. Müller, First order ferromagnetic transition in binary $CeIn_2$, Phys. Rev. B **80**, 184413 (2009).

[45] A. Steppke, R. Küchler, S. Lausberg, E. Lengyel, L. Steinke, R. Borth, T. Lühmann, C. Krellner, M. Nicklas, C. Geibel, F. Steglich, M. Brando, Ferromagnetic Quantum Critical Point in the Heavy-Fermion Metal $YbNi_4(P_{1-x}As_x)_2$, Science **339**, 933 (2013).

[46] N. Tateiwa, T. D. Matsuda, Y. Haga, and Z. Fisk, Pressure-induced ferromagnetism with strong Ising-type anisotropy in $YbCu_2Si_2$ Phys. Rev. B **89**, 035127 (2014).

[47] S. Viola Kusminskiy, K. S. D. Beach, A. H. Castro Neto, and D. K. Campbell, Mean-field study of the heavy-fermion metamagnetic transition Phys. Rev. B **77**, 094419 (2008).

[48] M. Bercx and F. F. Assaad, Metamagnetism and Lifshitz transitions in models for heavy fermions, Phys. Rev. B **86**, 075108 (2012).

[49] N. Perkins, J. Iglesias, M. Núñez-Regueiro, B. Coqblin, Coexistence of ferromagnetism and Kondo effect in the underscreened Kondo lattice, Europhys. Lett. **79**, 57006 (2007).

[50] F. Hardy, C. Meingast, V. Taufour, J. Flouquet, H. V. Löhneysen, R. A. Fisher, N. E. Phillips, A. Huxley, and J. C. Lashley, Two magnetic Grüneisen parameters in the ferromagnetic superconductor UGe_2, Phys. Rev. B **80**, 174521 (2009).

[51] V. Taufour, D. Aoki, G. Knebel, and J. Flouquet, Tricritical Point and Wing Structure in the Itinerant Ferromagnet UGe_2, Phys. Rev. Lett. **105**, 217201 (2010).

[52] H. Kotegawa, V. Taufour, D. Aoki, G. Knebel, and J. Flouquet, Evolution toward Quantum Critical End Point in UGe_2, J. Phys. Soc. Jpn. **80**, 083703 (2011).

[53] D. Aoki, K. Ishida, and J. Flouquet, Review of U-based Ferromagnetic Superconductors: Comparison between UGe_2, URhGe, and UCoGe, J. Phys. Soc. Jpn. **88**, 022001 (2019).

[54] M. Brando, D. Belitz, F. M. Grosche, and T. R. Kirkpatrick, Metallic quantum ferromagnets, Rev. Mod. Phys. **88**, 025006 (2016).

[55] B. H. Bernhard and J. Steinbach, Magnetocaloric effect in itinerant magnets around a metamagnetic transition, J. Magn. Magn. Mater. **441**, 49 (2017).

[56] M. Shimizu, Itinerant electron metamagnetism, J. Phys. (France) **43**, 155 (1982).

[57] H. Yamada, Metamagnetic transition and susceptibility maximum in an itinerant-electron system Phys. Rev. B **47**, 11211 (1993).

[58] D. Belitz, T. R. Kirkpatrick, and J. Rollbüler, Tricritical Behavior in Itinerant Quantum Ferromagnets, Phys. Rev. Lett. **94**, 247205 (2005).

[59] I. Giannakis, D. Sar, J. Friedman, Chang-Jong Kang, M. Janoschek, P. Das, E. D. Bauer, G. Kotliar, and P. Aynajian, Coexisting Kondo hybridization and itinerant *f*-electron ferromagnetism in UGe_2, Phys. Rev. Research **4**, L022030 (2022).

[60] M. M. Wysokiński, M. Abram, and J. Spałek, Criticalities in the itinerant ferromagnet UGe_2, Phys. Rev. B **91**, 081108(R) (2015).

[61] V. Taufour, U. S. Kaluarachchi, and V. G. Kogan, Constraints on the merging of the transition lines at the tricritical point in a wing-structure phase diagram, Phys. Rev. B **94**, 060410(R) (2016).

[62] T. R. Kirkpatrick and D. Belitz, Third Law of Thermodynamics and The Shape of the Phase Diagram for Systems with a First-Order Quantum Phase Transition, Phys. Rev. Lett. **115**, 020402 (2015).